

ACIS Memo #207
Massachusetts Institute of Technology
Kavli Institute for Astrophysics and Space Research
Cambridge, MA 02139
Room NE80-6053
cgrant@space.mit.edu

To: ACIS Team, CXC SOT and FOT teams
From: Catherine Grant
Subject: Consequences of a future unprotected radiation belt transit by ACIS
Date: 30 January 2007

Summary:

As the Chandra orbit evolves, the expected dose from an unprotected radiation belt passage changes, as does the predicted performance degradation. At the time of writing, the predicted dose is close to minimum, however over the next six to seven years the predicted dose increases by more than an order of magnitude. The change in front-illuminated (FI) CCD CTI and pulseheight for a single unprotected radiation belt passage from 1999 through 2026 is shown in Figure 6 and Table 4. The predicted $\delta\text{CTI/orbit}$ ranges from 4×10^{-7} to 8×10^{-6} at 5.9 keV and -120C (compared to the current slow increase of $\sim 3.2 \times 10^{-6}/\text{year}$). The predicted $\delta\text{PHA/orbit}$ for the top of the CCD (where the effects of CTI are largest) ranges from 0.04% to 0.8% at 5.9 keV and 0.08% to 1.4% at 1.5 keV. Higher focal plane temperatures will yield larger predicted CTI and pulseheight changes. In most years the predicted change is enough to require a recalibration of the FI CCD gain, and in the worst cases requires a complete recalibration of the CTI correction. The back-illuminated CCD CTI increase is a few percent or less of the FI CCD CTI increase. Inserting the HETG reduces the damage due to the protection of the polyimide support structure against low energy protons and no damage was measured during an HETG-protected radiation belt passage. The measured $3\text{-}\sigma$ upper limit on $\delta\text{CTI/orbit}$ with the HETG inserted is 44% of the predicted damage without the HETG. The LETG does *not* provide the same protection as the HETG. Temporal enhancements and orbit-to-orbit variations in the trapped-proton intensity are estimated to be no more than a factor-of-three over the predictions used above.

1 Introduction

This memo summarizes our flight experience with unprotected radiation belt transits and extrapolates this experience to the future. Section 2 presents the available ACIS data and analysis of CCD performance changes during the radiation belt transits in 1999. The evolution of Chandra's orbit and how this effects the expected dosage from radiation belt transits is described in Section 3. Shorter timescale temporal variations are discussed in Section 4. We conclude with Section 5 which contains our best estimate of the performance degradation from radiation belt transits as a function of time.

Table 1: 1999 Observation Timetable

Time	ObsID	FP Temp (deg C)	t_{exp} (ksec)
225:1500		Rad Belt Entry – ACIS-S	
228:0727		Rad Belt Entry – ACIS-S	
231:0230		Rad Belt Entry – “Safe”	
233:1326		Rad Belt Entry – ACIS-S	
236:0550		Rad Belt Entry – ACIS-I	
238:2013		Rad Belt Entry – ACIS-I	
241:1154		Rad Belt Entry – ACIS-S+HETG	
244:0407		Rad Belt Entry – HRC-I	
246:1833		Rad Belt Entry – HRC-I	
249:1026		Rad Belt Entry – HRC-S	
252:0225		Rad Belt Entry – ACIS-I	
252:2252	62411	–99.5	1.3
254:0836	62401	–109.2	2.4
254:1656		Rad Belt Entry – ACIS-S	
255:0900	62428	–99.5	3.3
255:2143	62425	–118.9	3.6
256:0907		Start +30C Bakeout	
257:0256	62418	–99.4	14.6
257:0857		Rad Belt Entry – ACIS-S	
259:2000	62537	–109.2	8.6
260:0034		Rad Belt Entry – ACIS-S+HETG	
260:1904	62535	–109.2	3.2
261:1501	62534	–109.2	3.8
261:1701	62533	–100.9	3.9
261:1901	62532	–89.8	3.9
261:2101	62531	–79.7	3.9
261:2301	62530	–69.7	3.8
262:0101	62529	–59.5	3.6
262:1226	1304	–109.2	7.9
262:1518		Rad Belt Entry – HRC-S	
263:0151	1306	–109.2	7.9

2 Flight experience with unprotected radiation belt transits

Between August 12 and September 18, 1999 (1999:224–261), Chandra went through eight radiation belt transits with ACIS in the focal plane. This resulted in substantial radiation damage to the eight front-illuminated (FI) CCDs. No damage was seen in the two back-illuminated (BI) CCDs. It is now understood that the damage was due to low energy protons (~ 100 keV) in the Earth’s radiation belts which scatter off the HRMA mirrors onto the focal plane. These protons are energetic enough to pass through the optical blocking filter and the CCD gate structures and interact in the depletion region and in the buried transfer channel of the FI CCDs, but not energetic enough to reach the buried transfer channel of the BI CCDs which is protected by ~ 40 μm of silicon. Similarly the framestore array was not damaged because of the few millimeters of gold-plated aluminum in the framestore cover. Chandra also went through two radiation belt transits with ACIS in the focal plane and the HETG inserted and one radiation belt transit with ACIS at a “safe” midpoint position without any apparent damage to the CCDs.

Table 1 shows a time history of radiation belt passages and ACIS external calibration source observations. The focal plane instrument is listed for each radiation belt passage as well as the presence of the HETG, if inserted. The ObsID, average focal plane temperature, and exposure time are given for each observation. The calibration source observations were all done in a standard faint mode with only two CCDs, the FI CCD S2 and the BI CCD S3 and a frametime of 3.2 seconds. Our current strategy of monitoring the ACIS calibration source twice each orbit was not yet in place during this period, so we cannot uniquely measure the performance change from each radiation belt passage. We will assume that the dosage received from each belt transit is approximately equal, but will revisit this assumption later. Observations were made at multiple focal plane temperatures (-60C to -120C) and bracket a room temperature bakeout ($+30\text{C}$) which produces additional performance changes. To isolate the performance changes due to additional radiation damage alone, our analysis must compare same-temperature observations and must not encompass the bakeout.

Table 2 lists the pairs of observations that we use to measure performance changes. In addition to the flight data listed in Table 1, we also use data taken before launch during thermal vacuum testing at Ball Aerospace at -110C (ISIM T/V) and during CCD level testing at MIT at -120C (MIT Lab) for comparison. The MIT lab data was taken before the CCDs were installed in the ACIS flight camera so the control and monitoring of CCD temperature was different and an ^{55}Fe source was used instead of the ACIS calibration source (^{55}Fe with Al and Ti fluorescence targets). Small differences due to temperature or spectral variations should be expected and, where possible, the ISIM T/V data is used instead. There is also a gain change between both sets of ground data and the flight data. We remove this gain change using some simple assumptions about the spatial and spectral properties of the pulseheight dependence of charge transfer inefficiency (CTI). Since the initial undamaged performance of the FI CCDs is nearly independent of temperature over the range -100C to -120C , ground data can be used as a comparison to flight data at many temperatures. This is not the case for the initial performance of the BI CCDs, which changes significantly over this range. We have increased the measurement errors to account for small differences in the temperature between the comparison observations equivalent to temperature deviations of 0.4C for MIT Lab data and 0.1C otherwise. All data have been corrected to the nominal temperature reading for each temperature set point of -100C (-99.5C), -110C (-109.2C) and -120C (-119.9C)¹. For more on the dependence of ACIS CTI on temperature see <http://space.mit.edu/~cgrant/ctitemp>.

We also compare the ground data to flight data taken during two weeks in early 2000. In this case

¹What I label as “ -120C ” data is actually equivalent to the standard (since January 2000) set point of -121C . This is consistent with the colloquial usage.

Table 2: Comparison Observations

Before	Temp (deg C)	After	Temp (deg C)	Num. of RadBelts	
<u>FI CCD S2</u>					
ISIM T/V	-109.0	ObsID 62411	-99.5	6	
ISIM T/V	-109.0	ObsID 62428	-99.5	7	
ObsID 62411	-99.5	ObsID 62428	-99.5	1	
ISIM T/V	-109.0	ObsID 62401	-109.2	6	
ISIM T/V	-109.0	ObsID 62425	-118.9	7	
ObsID 62537	-109.2	ObsID 62535/62534	-109.2	1	HETG inserted
ISIM T/V	-109.0	Jan 2000	-119.8	8	includes bakeout
<u>BI CCD S3</u>					
ObsID 62411	-99.5	ObsID 62428	-99.5	1	
ISIM T/V	-109.0	ObsID 62401	-109.2	6	
MIT Lab	-120	ObsID 62425	-118.9	7	
ObsID 62537	-109.2	ObsID 62535/62534	-109.2	1	HETG inserted
MIT Lab	-120	Jan 2000	-119.8	8	includes bakeout

the accumulated damage includes all eight radiation belt passages, the room temperature bakeout, and the much smaller irradiation outside of the belts between September 1999 and January 2000. No adjustments were made to correct for these additional effects, so these results can be considered upper limits to the damage from radiation belt passages alone.

Table 3 and Figure 1 present the average performance change from a single radiation belt passage in 1999 for each CCD type and focal plane temperature. Our primary metric for measuring radiation damage on ACIS is charge transfer inefficiency (CTI) at the Mn-K α line (5.9 keV). CTI is the fractional charge loss per pixel and is measured here in the same way as in our CTI monitoring program. Currently the parallel CTI on the ACIS FI CCDs ranges from $1 - 2 \times 10^{-4}$ and from $2 - 3 \times 10^{-5}$ for the BI CCDs. The reason for the variation of FI CTI across the focal plane is not understood but is likely a result of non-uniform irradiation. The S2 CCD used here is near the middle of this range, so if future radiation belt passages follow the same non-uniformity pattern, the damage to the I-array CCDs will be 20–30% smaller than these estimates. Through careful management of radiation exposure (safing during radiation belt passages and solar storms) the rate of CTI increase has been minimized to about 3×10^{-6} / year for FI CCDs and about 1×10^{-6} / year for BI CCDs. The CTI increase from a single radiation belt passage in 1999 ranges from 1.1 to 3.0×10^{-5} for FI CCDs and from 2×10^{-7} to less than 4×10^{-6} for BI CCDs depending on the focal plane temperature. Because the damage during radiation belt transits is due to low energy, weakly penetrating particles, the BI CCD CTI increase is a few percent or less of the FI CCD CTI increase. A single radiation belt passage like those in 1999 would produce the same CTI increase as about three and a half years of the current slow rate at -120C .

No damage is seen when the HETG is inserted with a $3\text{-}\sigma$ upper limit of 7.6×10^{-6} for FI CCDs at -110C , i.e., $< 44\%$ of that expected with the HETG retracted. While we do not have any data with the LETG inserted, we believe that it would *not* provide the same protection as

Table 3: Performance Change from a Single Radiation Belt Passage in 1999

Temp (deg C)	δ CTI ($\times 10^{-5}$)		δ PHA (%)		δ FWHM (eV)	
	5.9 keV	1.5 keV	5.9 keV	1.5 keV	5.9 keV	1.5 keV
FI CCD						
-100	3.01 ± 0.04	4.40 ± 0.11	2.78 ± 0.04	4.93 ± 0.14
-110	1.73 ± 0.02	2.70 ± 0.06	1.62 ± 0.01	3.00 ± 0.05	46 ± 2	23 ± 2
-120	1.14 ± 0.01	1.90 ± 0.03	1.10 ± 0.01	2.06 ± 0.02	21 ± 1	11 ± 1
BI CCD						
-100	< 0.40	< 1.80	< 0.27	< 0.94
-110	< 0.04	< 0.20	< 0.04	< 0.12
-120	0.02 ± 0.01	...	< 0.02
FI CCD with HETG inserted						
-110	< 0.76	< 2.39	< 0.48	< 1.48
FI CCD ground through 2000 (includes bakeout)						
-120	1.98 ± 0.01	3.66 ± 0.03	1.896 ± 0.004	3.87 ± 0.01	37.3 ± 0.1	20.4 ± 0.1
BI CCD ground through 2000 (includes bakeout)						
-120	0.019 ± 0.003	...	< 0.02

Note: δ PHA and δ FWHM are for the top 64 rows of the CCD, furthest from the framestore, where the effects of parallel CTI are largest. Results for δ PHA and δ FWHM are not listed where the performance is too degraded for reliable fits (i.e. -100C FI CCD), where the data do not exist (1.5 keV MIT Lab) or where there is no measured CTI change. Upper limits are $3\text{-}\sigma$.

the HETG. The HETG gratings are supported by a thin polyimide structure which absorbs and Rutherford scatters much of the damaging radiation while the LETG gratings are free-standing. Ion-transport simulations, performed by Project Science, confirm that the HETG provides a high degree of protection against the damaging low-energy protons, whereas the LETG does not.

Table 3 also lists the change in pulseheight and spectral line width for the top 64 rows of the CCD, where the effects of CTI are largest. (The aimpoint in the ACIS-I configuration is near the top of the I3 FI CCD.) We do not list FWHM results for FI CCDs at -100C because the spectral performance is so poor that the lines are blended and our fits are unreliable. We also do not list FWHM results for cases which have only an upper limit to the change in CTI. The pulseheight decrease at the top of the CCD from a single radiation belt passage in 1999 ranges from 1–5% for FI CCDs depending on energy and temperature. Near the bottom of the CCD the pulseheight change approaches zero. The current calibration accuracy for pulseheight is 0.3% so this is considerably larger and would require recalibration. The FI CCD FWHM increase at the top of the CCD from a single radiation belt passage in 1999 ranges from 21–46 eV at 5.9 keV and 11–23 eV at 1.5 keV depending on temperature. The current FWHM at -120C is about 450 eV and 250 eV at 5.9 and 1.5 keV, so this represents an increase of 5% and 4%.

We have assumed in this analysis that the fluence from all eight radiation belt passages in 1999 is roughly the same. This is not necessarily the case since the magnetosphere can vary on time scales less than a Chandra orbit and each orbit will intersect different portions of the magnetosphere. We can roughly quantify this variation by examining ObsID 62411 and 62428 which were taken one orbit apart. For the six belt passages between measurements on the ground and ObsID 62411 the

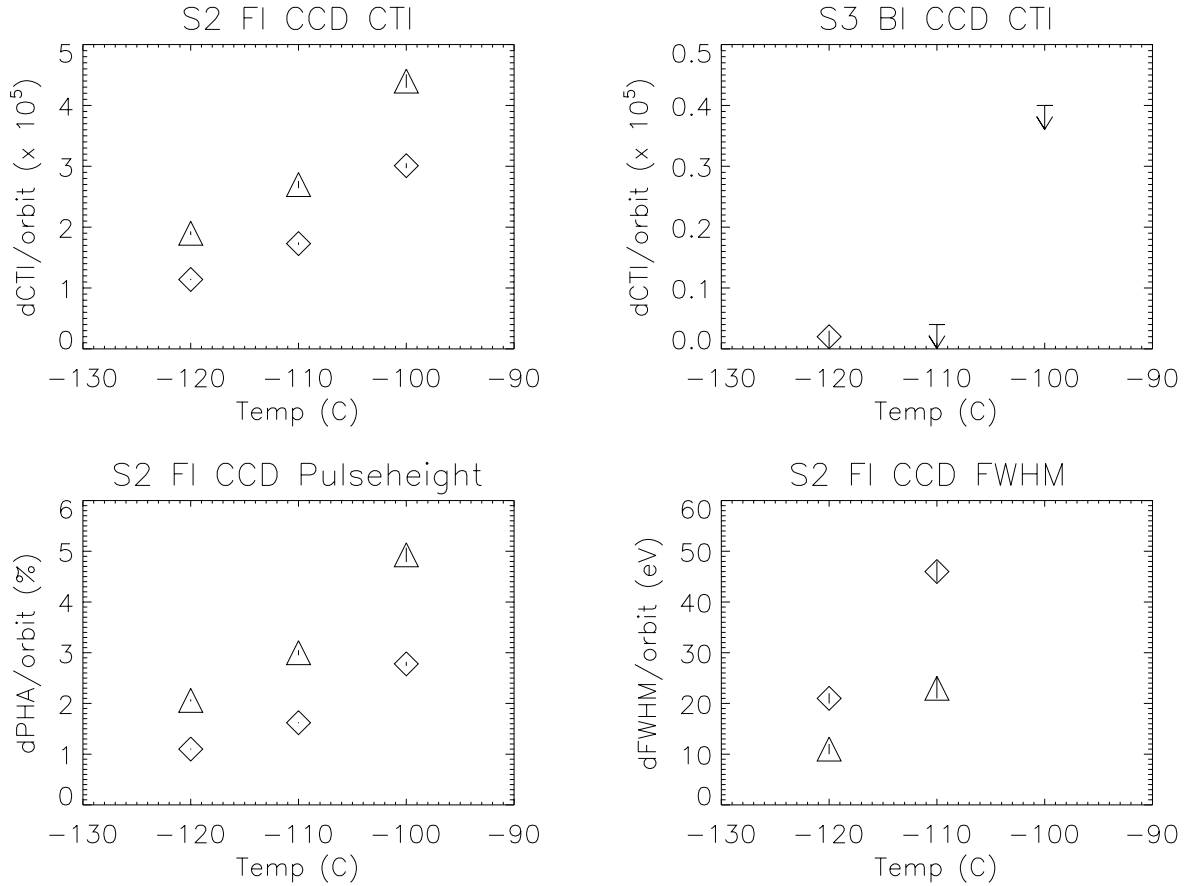


Figure 1: Average performance change from a single radiation belt passage in 1999. The top panels show the change in CTI per orbit for the FI (left) and BI (right) CCDs at 1.5 keV (triangles) and 5.9 keV (diamonds). Only 5.9 keV is shown for the BI CCD because of the better statistics. The bottom panels show the change of pulseheight in percent and FWHM in eV for the top 64 rows of the FI CCD, where the effects of parallel CTI are largest. The vertical lines are the 1-sigma error bars. The upper limits are 3σ .

average CTI increase per orbit was $(3.09 \pm 0.08) \times 10^{-5}$. The CTI increase from one additional belt passage between 62411 and 62428 was $(2.3 \pm 0.6) \times 10^{-5}$ — i.e., 0.74 ± 0.19 of the average. Interestingly, an orbit-by-orbit analysis of the AP8-predicted fluence finds a similar ratio — namely, 0.65 — of the fluence of the 7th ACIS-exposure perigee pass to the average of the first 6. However, this agreement is somewhat fortuitous in that true temporal variations in the proton-belt intensity can also occur.

An additional performance parameter that can be affected by increasing CTI is detection efficiency. Changing CTI can induce changes in the grade distribution such that real X-ray events are morphed into grades that are more representative of cosmic ray events and are thus discarded. This is generally a few percent effect. A larger effect occurs when the pulseheight decrease from CTI approaches the event threshold (39 ADU for FI CCDs) at the highest row numbers. These events are rejected on-board and cannot be recovered. Using some simple assumptions about the dependence of line pulseheight and width on CTI, we estimate that for line energies of 500 eV,

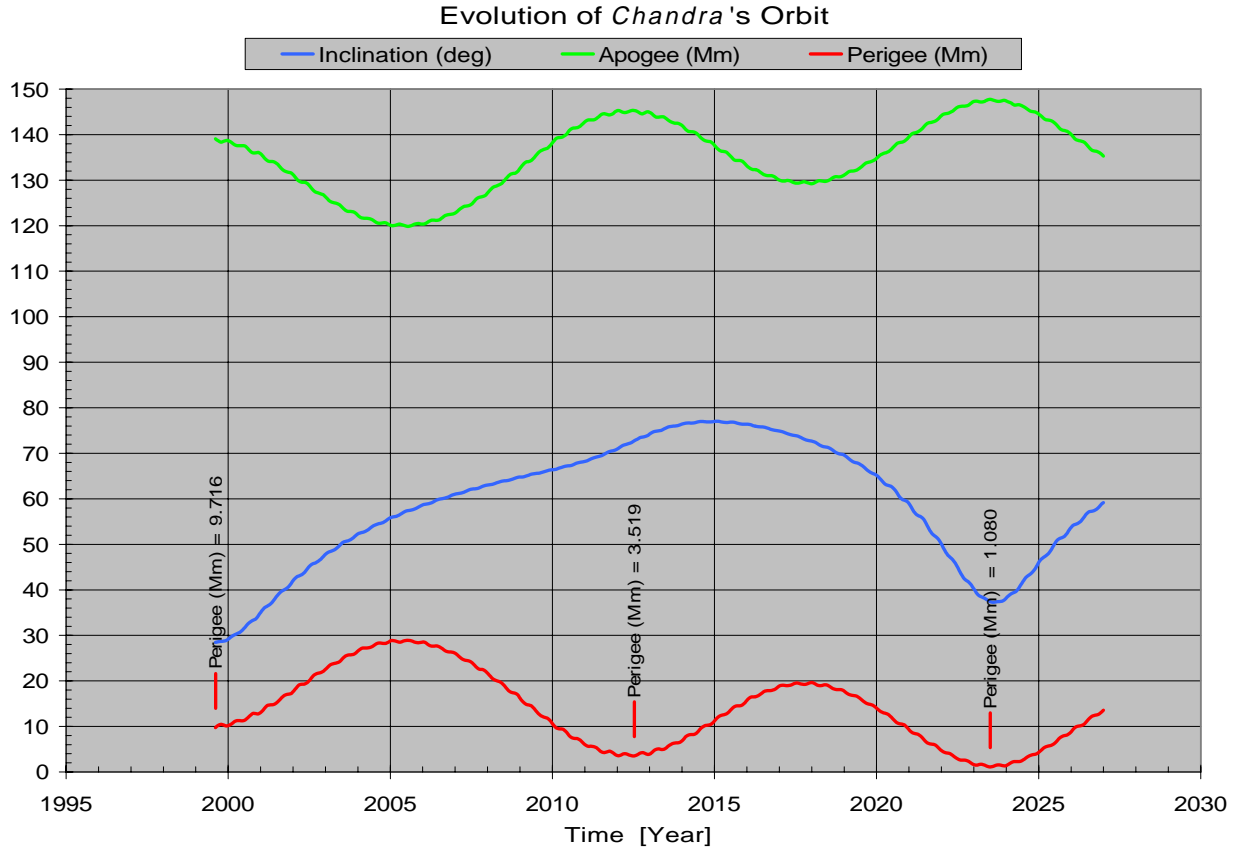


Figure 2: Evolution of Chandra’s orbital apogee, perigee and inclination from August 1999 through December 2026. Apogee and perigee are measured in Megameters (10^6 m) and inclination in degrees. Plot courtesy of Project Science (MSFC) based on orbital ephemeris data provided by Eric Martin (NGST).

1.5 keV and 5.9 keV, the line center in the top 64 rows reaches the event threshold at CTI levels of 3.1×10^{-4} , 6.5×10^{-4} , and 1.2×10^{-3} , respectively. From the current CTI of 1.8×10^{-4} and the CTI increase from a single belt passage in 1999 of 1.1×10^{-5} , it would take tens of unprotected passages to reach these levels at which approximately half of the redistribution function would be below the threshold. A more restrictive limit is when the $3\text{-}\sigma$ line width intersects the event threshold. Currently, the width of the 500 eV line is just grazing the event threshold on S2. Any additional radiation damage would involve some small loss of low energy detection efficiency at the top of the S2 CCD. We estimate that for line energies of 1.5 keV and 5.9 keV, the $3\text{-}\sigma$ line width in the top 64 rows reaches the event threshold at CTI levels of 4.1×10^{-4} and 8.0×10^{-4} , respectively, which again represents tens of unprotected “1999 equivalent” passages.

3 Orbit evolution and predictions of radiation belt dosage

Chandra is in a highly elliptical orbit in which both the orbital eccentricity and inclination evolve with time due primarily to interactions with the Moon. A consequence is that the perigee and apogee altitudes vary quasi-sinusoidally with an approximate period of 12 years. Figure 2 shows the orbit apogee, perigee, and inclination as a function of time from launch through the end of 2026. Due to the variation in perigee and inclination, Chandra’s exposure to the radiation belts

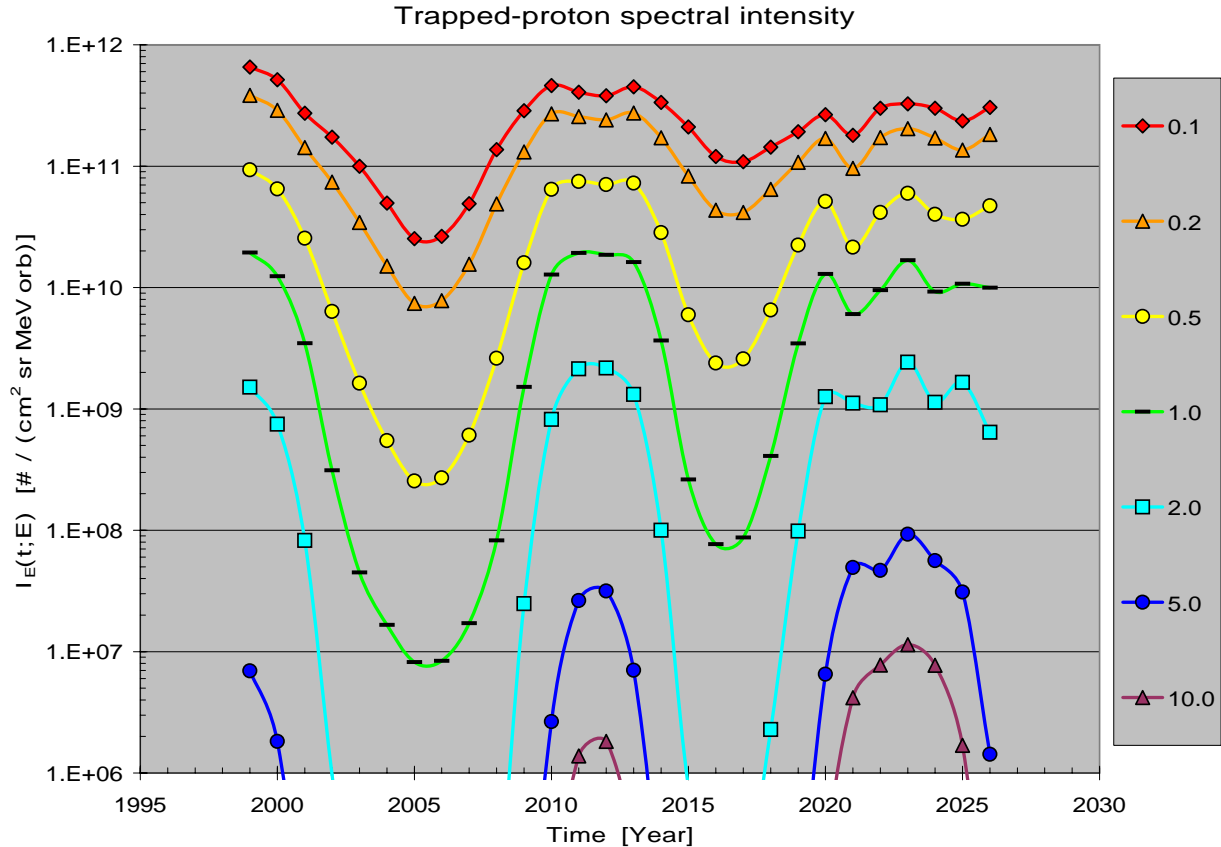


Figure 3: Evolution of Chandra’s trapped-proton spectral-intensity ($p/(\text{cm}^2 \text{ sr MeV orbit})$) time dependence from 1999 through 2026 for energies from 100 keV to 10 MeV. The legend on the right indicates the color/symbol combination for each energy in MeV. Plot courtesy of Project Science (MSFC).

changes substantially. Maximum exposure occurs around perigee minima in 1999 (9.716 Mm), 2012 (3.519 Mm), and 2023 (1.080 Mm). Since the radiation belts are not spherically symmetric, this exposure is also affected by the changing inclination.

Using the long-term Chandra orbital ephemeris, Project Science (MSFC) computed the external fluence of trapped protons using the SPENVIS tool to propagate the orbit in a standard AP8 environment (Project Science memo dated 2006.01.13). Each data point represents a 20-orbit SPENVIS simulation starting in mid-August of each year at 1-year intervals. For Chandra’s 63.5 hour orbital period, each run then spans 52.9 days. The radiation environment is the standard AP8 model for trapped protons — AP8-Max for 1999–2003, 2010–2014, and 2021–2025; AP8-Min for other periods. (For high earth orbits such as Chandra’s, AP8-Max and AP8-Min give essentially the same fluence). Figure 3 shows the trapped-proton spectral intensity as a function of time at energies from 100 keV to 10 MeV. Figures 4 and 5 are the spectral-intensity spectra for 1999 through 2012 and 2013 through 2026. The orbital modulation is quite apparent with maximum trapped proton fluence around 1999, 2012, and 2023 corresponding to minima in orbit perigee. Exposure to hard protons increases with each successive perigee minima as the orbit transits the more interior regions of the radiation belts which trap the higher-energy protons. At the most damaging proton energies ($\sim 100 \text{ keV}$), the highest intensity levels occurred at launch followed by the lowest levels in 2005. The future prediction is for more moderate levels. For more details on Chandra radiation

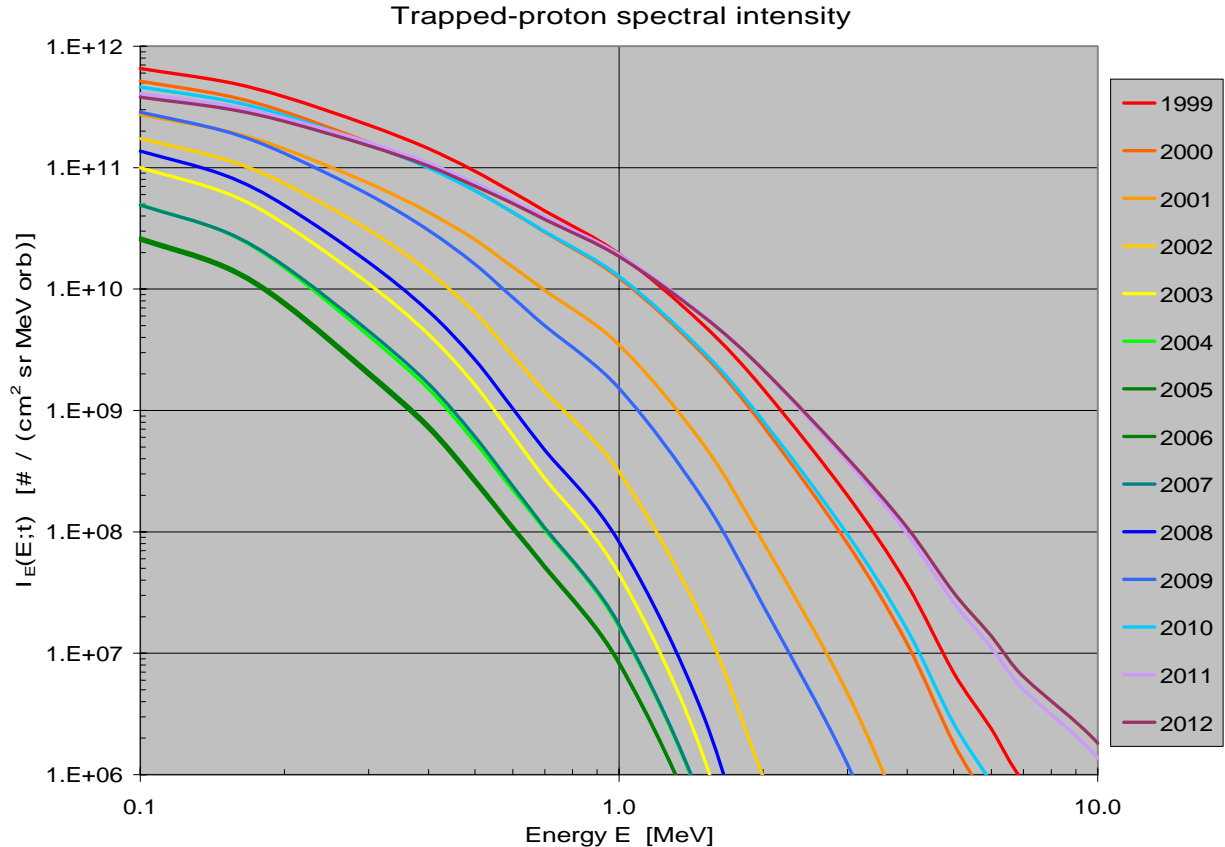


Figure 4: Evolution of Chandra’s trapped-proton spectral intensity ($p/(\text{cm}^2 \text{ sr MeV orbit})$) for the years 1999 through 2012. The legend on the right indicates the color designation for each year. Plot courtesy of Project Science (MSFC).

modelling, see O’Dell et al. (2005, Proc. SPIE, 5898, 212) and the references therein.

4 Temporal variations in proton fluence on shorter timescales

In the previous section we presented the evolution of the trapped-proton fluence on long-time scales where each data point represented an average of 20-orbits at 1-year intervals. Given the variation in geomagnetic activity on much shorter timescales (i.e. days), one might expect proportionate changes in the proton fluence. In addition, orbit-to-orbit differences in fluence can result from the rotation of the Earth and its asymmetric magnetic field. The expected short-term variations about the standard AP8 proton fluence model are described in memos dated 2006.10.31 and 2006.12.04 by Project Science and are summarized below.

The AP8 model of the proton fluence accurately estimates the long-term-average (mean) fluence. Temporal changes in the trapped-proton intensity correspond to proportionate changes in the ring current, which perturbs the earth’s magnetic field during geomagnetic storms. The temporal variations in orbital proton fluence are estimated to be about a factor of two (geomagnetic quiet) up to four (geomagnetic active).

The orbit-to-orbit fluence differences due to the rotation of the Earth and its asymmetric magnetic field are generally small — less than a factor of 2 between two orbits, much less than this when averaged over 3 successive orbits (because the orbit’s period is close to $8/3$ days). Larger

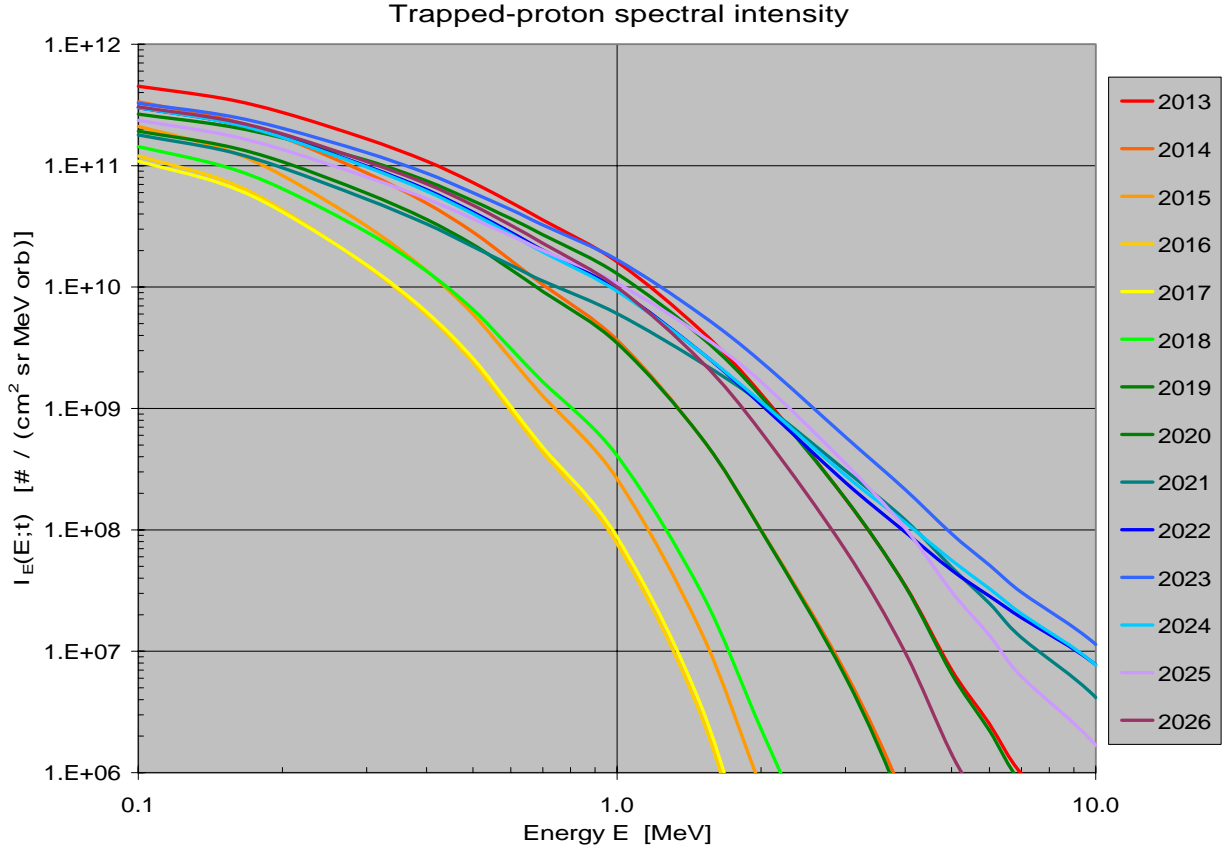


Figure 5: Evolution of Chandra’s trapped-proton spectral intensity ($p/(\text{cm}^2 \text{ sr MeV orbit})$) for the years 2013 through 2026. The legend on the right indicates the color designation for each year. Plot courtesy of Project Science (MSFC).

orbit-to-orbit fractional changes occur during epochs for which the Chandra orbit only partially penetrates the trapped-proton belt. In these cases, however, the proton orbital fluence is also very low. Note that this “uncertainty” is deterministic — i.e., given a specific date, we can compute the AP8-estimated fluence for the corresponding orbit. As discussed in Section 2, the measured $\delta\text{CTI}/\text{orbit}$ variation in 1999 is consistent with this rotational modulation of the fluence.

We recommend a factor-of-3 margin over the fluence estimates previously presented, in order to allow for temporal enhancements in the trapped-proton intensity. This factor-of-3 margin represents a 99%-confidence limit over the mean fluence calculated for a specific orbit and a 95%-confidence limit for an annually-averaged orbit. The factor-of-3 margin has not been incorporated into the following discussion.

5 Radiation belt performance degradation as a function of time

Given the evolution of the Chandra radiation environment and the measured performance degradation of the CCDs in 1999, we can extrapolate this degradation to future unprotected radiation belt passages. We initially assume a mono-energetic 100 keV proton spectrum, but will re-address and justify this assumption later. We will also assume the current focal plane temperature of -120C . As was shown in Section 2, the magnitude of the performance degradation is dependent on the operating temperature. While there are no plans currently to change the nominal CCD operating

temperature, it may be necessary to increase the set point at some future time to maintain temperature stability. The results of Table 3 can be used to roughly scale our predictions to other temperatures.

Figure 6 and Table 4 present the predicted CTI and pulseheight change for a single unprotected radiation belt passage as a function of time. The size of the CTI increase varies widely from a maximum of 1.1×10^{-5} at launch to a minimum of 4.3×10^{-7} around 2005–2006 or 6% down to 0.2% of the current CTI. The equivalent in years of the measured slow increase of CTI is shown in the right axis and ranges from almost four years to as little as two months. Typical errors on single observation CTI measurements are currently a little below 1×10^{-6} so the smallest increases would be difficult to measure without longer baselines and careful analysis. The percent change in pulseheight for the top 64 rows of the CCD at 1.5 keV and 5.9 keV is also shown in Figure 6 and Table 4. Since charge loss $\sim \sqrt{E}$, the magnitude of the pulseheight change (in percent) will increase with decreasing energy. The pulseheight change ranges from 0.08% to 2% at 1.5 keV and from 0.04% to 1.1% at 5.9 keV.

Thus far we have assumed a 100 keV mono-energetic incident proton spectrum. This is consistent with lab measurements of low energy proton damage on ACIS CCDs which have shown that the CTI change per unit proton fluence goes roughly as $E^{-1.68}$ from approximately 100 keV to 400 keV with a sharp drop-off at energies below 100 keV and is roughly flat from 400 keV through 40 MeV (Bautz, MIT ACIS internal memo, 29 October 1999, available at CXC ACIS Internal website). From the spectral intensity data we can see that the proton spectrum changes throughout this time period, so consideration of a larger energy band may be warranted. Thus far we have considered only the external fluence; the fluence at the focal plane is the product of the external fluence (p / (cm² sr MeV)) and the acceptance (external cm² sr per focal plane cm²). We adopt the acceptance energy dependence shown in Figure 5 of Kolodziejczak et al. (2000, Proc. SPIE, 4140, 135) who model the scattering and transmittance of the HRMA. The acceptance peaks at ~ 1 MeV, a much higher energy than the ~ 100 keV peak of the CTI damage. Given the focal plane fluence and the energy dependence of CTI damage, and normalizing to the known damage in 1999, we can integrate over proton energy (100 keV–10 MeV) to predict the full spectrum CTI degradation as a function of time, i.e. $CTI = \int x(E) \alpha(E) \delta CTI(E) dE$ where $x(E)$ is the external fluence, $\alpha(E)$ is the acceptance and $\delta CTI(E)$ is the change in CTI per unit fluence. Due to the strong decline of CTI damage with increasing proton energy and the steep spectrum of the orbit-averaged external fluence of protons, the full spectrum CTI evolution is always within 5×10^{-7} of the 100 keV mono-energetic case, so our original simplification is valid.

5.1 Need for re-calibration

The horizontal dashed line in Figure 6 indicates the 0.3% gain calibration baseline. Except for the period from mid-September 2003 through mid-February 2008, a single unprotected passage would at least require gain recalibration. This type of recalibration is currently performed every three months to correct for the gain time-dependence due to slowly increasing CTI. Calibration involving the inputs to the CTI corrector is much more time-consuming and has only been done twice for data at -120 C, for the time period January 2000 through August 2002 and for August 2002 through the present. The change in CTI during this 2000–2002 time period is approximately 1×10^{-5} , so except for the period immediately after launch, no single belt passage would require this type of recalibration. In reality, the damage from the unprotected radiation belt passage is in addition to accumulated slow increase since the previous recalibration, so it is much more likely to be required. Assuming accumulated damage since the previous calibration of 5×10^{-6} , there are three approximate time periods which require CTI corrector recalibration after a single unprotected

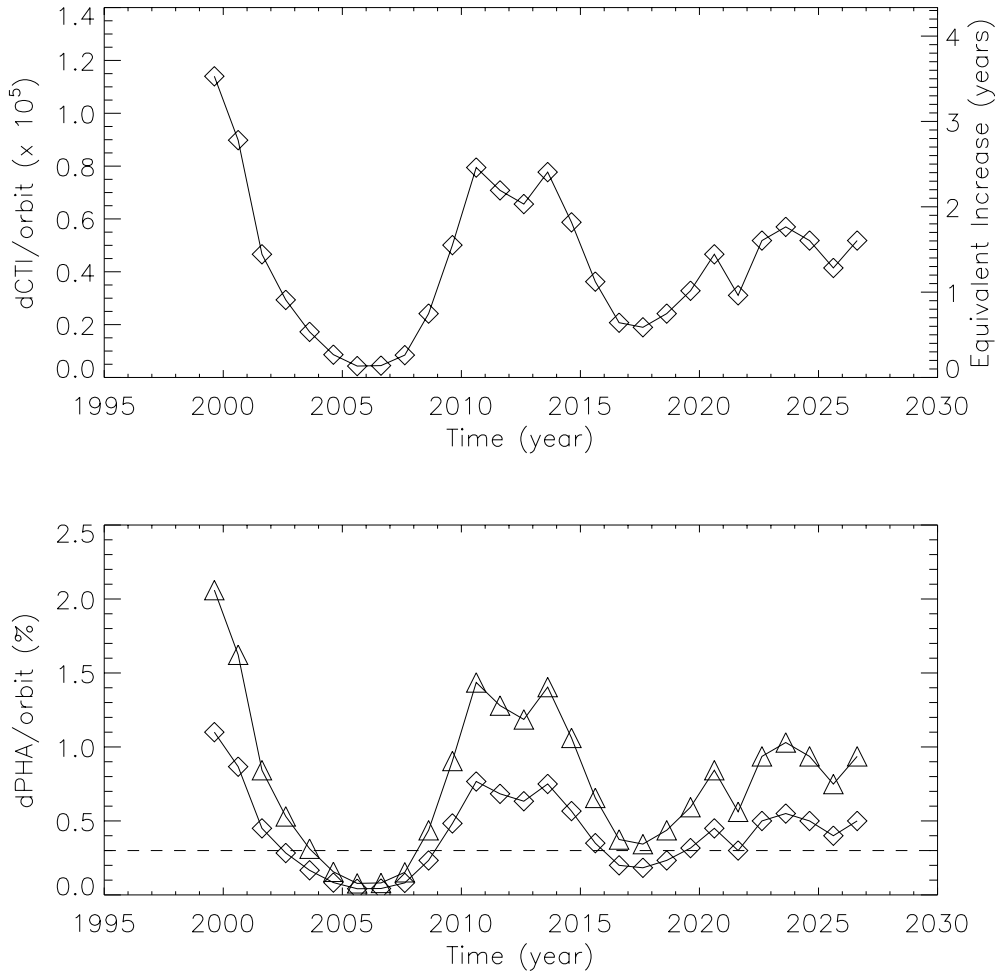


Figure 6: Performance change from a single radiation belt passage as a function of time at the current focal plane temperature of -120C . At higher focal plane temperatures the performance change is larger. The top panel shows the change in CTI per orbit for the S2 FI CCD at 5.9 keV. The right-axis of the plot shows the equivalent increase in years from the observed slow increase in CTI. The bottom panels show the change of pulseheight in percent at 1.5 keV (triangles) and 5.9 keV (diamonds) for the top 64 rows of the FI CCD, where the effects of parallel CTI are largest. The horizontal dashed line indicates the 0.3% gain accuracy goal of ACIS calibration.

Table 4: Performance Change from a Single Radiation Belt Passage as a Function of Time

Year	δCTI ($\times 10^{-5}$)	δPHA (%)		Equiv. ^a Years	Year	δCTI ($\times 10^{-5}$)	δPHA (%)		Equiv. ^a Years
		5.9 keV	1.5 keV				5.9 keV	1.5 keV	
1999	1.14	1.10	2.06	3.5	2013	0.78	0.75	1.40	2.4
2000	0.90	0.87	1.62	2.8	2014	0.59	0.57	1.06	1.8
2001	0.47	0.45	0.84	1.4	2015	0.36	0.35	0.66	1.1
2002	0.29	0.28	0.53	0.9	2016	0.21	0.20	0.37	0.6
2003	0.17	0.17	0.31	0.5	2017	0.19	0.18	0.34	0.6
2004	0.09	0.08	0.16	0.3	2018	0.24	0.23	0.44	0.7
2005	0.04	0.04	0.08	0.1	2019	0.33	0.32	0.59	1.0
2006	0.04	0.04	0.08	0.1	2020	0.47	0.45	0.84	1.4
2007	0.08	0.08	0.15	0.3	2021	0.31	0.30	0.56	1.0
2008	0.24	0.23	0.44	0.7	2022	0.52	0.50	0.94	1.6
2009	0.50	0.48	0.91	1.6	2023	0.57	0.55	1.03	1.8
2010	0.79	0.77	1.44	2.5	2024	0.52	0.50	0.94	1.6
2011	0.71	0.68	1.28	2.2	2025	0.41	0.40	0.75	1.3
2012	0.66	0.63	1.19	2.0	2026	0.52	0.50	0.94	1.6

^a Equivalent increase in years from the observed slow increase in CTI.

Note: Each data point is a 20-orbit average starting in mid-August of the listed year. The data is for a focal plane temperature of -120C ; higher focal plane temperatures will yield larger performance changes. δPHA is for the top 64 rows of the CCD, furthest from the framestore, where the effects of parallel CTI are largest.

radiation belt passage: launch through mid-July 2001, mid-August 2009 through early-January 2015, and mid-July 2022 through mid-October 2024.

6 Note

All of the figures and much of the text in sections 3 and 4 are taken from three Project Science memos by Steve O'Dell (MSFC) dated 2006.01.31, 2006.10.31, and 2006.12.04. The interested reader is encouraged to seek these out for more technical details and additional figures.